



Article

# An Innate Moving Frame on Parametric Surfaces: The Dynamics of Principal Singular Curves

Moody T. Chu 1,\* and Zhenyue Zhang 2

- Department of Mathematics, North Carolina State University, Raleigh, NC 27695-8205, USA
- <sup>2</sup> Department of Mathematics, Zhejiang University, Hangzhou 310027, China; zyzhang@zju.edu.cn
- \* Correspondence: mtchu@ncsu.edu

Abstract: This article reports an experimental work that unveils some interesting yet unknown phenomena underneath all smooth nonlinear maps. The findings are based on the fact that, generalizing the conventional gradient dynamics, the right singular vectors of the Jacobian matrix of any differentiable map point in directions that are most pertinent to the infinitesimal deformation of the underlying function and that the singular values measure the rate of deformation in the corresponding directions. A continuous adaption of these singular vectors, therefore, constitutes a natural moving frame that carries indwelling information of the variation. This structure exists in any dimensional space, but the development of the fundamental theory and algorithm for surface exploration is an important first step for immediate application and further generalization. In this case, trajectories of these singular vectors, referred to as singular curves, unveil some intriguing patterns per the given function. At points where singular values coalesce, curious and complex behaviors occur, manifesting specific landmarks for the function. Upon analyzing the dynamics, it is discovered that there is a remarkably simple and universal structure underneath all smooth two-parameter maps. This work delineates graphs with this interesting dynamical system and the possible new discovery that, analogous to the double helix with two base parings in DNA, two strands of critical curves and eight base pairings could encode properties of a generic and arbitrary surface. This innate structure suggests that this approach could provide a unifying paradigm in functional genetics, where all smooth surfaces could be genome-sequenced and classified accordingly. Such a concept has sparked curiosity and warrants further investigation.

**Keywords:** moving frame; nonlinear variation; gradient adaption; singular curves; critical curves; base pairings; parametric surfaces; geometric genome

MSC: 51N05; 37B35; 65L07; 37N30; 65D18; 53A05



Citation: Chu, M.T.; Zhang, Z. An Innate Moving Frame on Parametric Surfaces: The Dynamics of Principal Singular Curves. *Mathematics* **2023**, *11*, 3306. https://doi.org/10.3390/math11153306

Academic Editor: Takashi Suzuki

Received: 6 July 2023 Revised: 22 July 2023 Accepted: 24 July 2023 Published: 27 July 2023



Copyright: © 2023 by the authors. Licensee MDPI, Basel, Switzerland. This article is an open access article distributed under the terms and conditions of the Creative Commons Attribution (CC BY) license (https://creativecommons.org/licenses/by/4.0/).

#### 1. Introduction

The notion of nonlinear maps has been used in almost every field of discipline as the most basic apparatus to describe complicated phenomena. However, the metaphysical question of what impinges on a function (in such a way that we may make use of its variations to denote distinct episodes) remains a natural mystery. Surface descriptions and their constructions in  $\mathbb{R}^3$ , for example, are of critical importance to a wide range of disciplines. But what makes surfaces present so many different shapes and geometric properties? This paper reports a preliminary study of a dynamics system inbuilt into every function, which might suggest an alternative, interesting, and possibly universal paradigm to help explore these questions.

Our idea is motivated by gradient adaption, which is ubiquitous in nature. Heat transfer by conduction and the osmosis of substances are two prevalent examples. They illustrate this natural phenomenon, moving against the temperature gradient, which is perpendicular to the isothermal surfaces, and down a concentration gradient across the cell

Mathematics 2023, 11, 3306 2 of 20

membrane, without requiring energy use. Gradient adaption follows the fundamental fact that the gradient

$$\nabla \eta(\mathbf{x}) := \left[ \frac{\partial \eta}{\partial x_1}, \dots, \frac{\partial \eta}{\partial x_n} \right]$$

of a given smooth scalar function  $\eta: \mathbb{R}^n \longrightarrow \mathbb{R}$  points in the steepest ascent direction for the function value  $\eta(\mathbf{x})$  with the maximum rate exactly equal to the Euclidean norm  $\|\nabla \eta(\mathbf{x})\|$ . A mechanical generalization of the gradient of a scalar function to a smooth vector function  $\mathbf{f}: \mathbb{R}^n \longrightarrow \mathbb{R}^m$  should be the Jacobian matrix defined by

$$\mathbf{f}'(\mathbf{x}) := \left[ egin{array}{ccc} rac{\partial f_1}{\partial x_1} & \dots & rac{\partial f_1}{\partial x_n} \ dots & \ddots & dots \ rac{\partial f_m}{\partial x_1} & \dots & rac{\partial f_m}{\partial x_n} \end{array} 
ight].$$

In this situation, the information about how f(x) transforms itself is masked by the combined effect of m gradients. One way to quantify the variation of f is to measure the rate of change along any given unit vector  $\mathbf{u}$  via the norm of the directional derivative

$$\lim_{t\to 0} \left\| \frac{\mathbf{f}(\mathbf{x} + t\mathbf{u}) - \mathbf{f}(\mathbf{x})}{t} \right\| = \|\mathbf{f}'(\mathbf{x})\mathbf{u}\|,\tag{1}$$

where in this discussion, we limit ourselves to the standard Euclidean norm only. Similar to the gradient adaption, we look at which directions function f(x) changes most rapidly and how much the maximum rate is attained. The answer lies in the notion of the singular value decomposition (SVD) of the Jacobian matrix f'(x).

Any given matrix  $A \in \mathbb{R}^{m \times n}$  enjoys a factorization of the form

$$A = V \Sigma U^{\top}, \tag{2}$$

where  $V \in \mathbb{R}^{m \times m}$  and  $U \in \mathbb{R}^{n \times n}$  are orthogonal matrices,  $\Sigma \in \mathbb{R}^{m \times n}$  is zero everywhere except for the nonnegative elements  $\sigma_1 \geq \sigma_2 \geq \ldots \geq \sigma_\kappa > \sigma_{\kappa+1} = \ldots = 0$  along the leading diagonal, and  $\kappa = \operatorname{rank}(A)$ . The scalars  $\sigma_i$  and corresponding columns  $\mathbf{u}_i$  in U and  $\mathbf{v}_i$  in V are called singular values, and the right and left singular vectors of A, respectively [1]. The notion of the SVD has long been conceived in various disciplines [2] as it appears frequently in a remarkably wide range of important applications, e.g., data analysis [3], dimension reduction [4], signal processing [5], image compression, principal component analysis [6], to name a few. Among the multiple ways to characterize the SVD of a matrix A, the variational formulation, i.e., solving the problem

$$\max_{\|\mathbf{u}\|=1} \|A\mathbf{u}\|,\tag{3}$$

sheds light on an important geometric property of the SVD. One can show that the unit's stationary points,  $\mathbf{u}_i \in \mathbb{R}^n$  for problem (3), and the associated objective values,  $\|A\mathbf{u}_i\|$ , are exactly the right singular vectors and the singular values of A. By duality, there exists a unit vector  $\mathbf{v}_i \in \mathbb{R}^m$ , such that  $\mathbf{v}_i^\top A \mathbf{u}_i = \sigma_i$ . This  $\mathbf{v}_i$  is the corresponding left singular vector of A. Because the linear map A transforms the unit sphere in  $\mathbb{R}^n$  into a hyperellipsoid in  $\mathbb{R}^m$ , the right singular vectors,  $\mathbf{u}_i$ s, are the pivotal directions that are mapped to the semi-axis directions of the hyperellipsoid. Upon normalization, these semi-axis directions are precisely the left singular vectors  $\mathbf{v}_i$ 's. Additionally, the singular values measure the extent of deformation. In this way, it is, thus, understood that the SVD of the Jacobian matrix  $\mathbf{f}'(\mathbf{x})$  carries crucial information about the infinitesimal deformation property of the nonlinear map  $\mathbf{f}$  at  $\mathbf{x}$ . At every point  $\mathbf{x} \in \mathbb{R}^n$ , we now have a set of orthonormal vectors that point in directions that are pertinent to the variation of  $\mathbf{f}$ . These orthonormal vectors form a natural frame, point-by-point.

Mathematics 2023, 11, 3306 3 of 20

In nature, a system often adapts itself continuously in the gradient direction. Thus, we are inspired to believe that tracking down the "motion" of these frames might help reveal some innate peculiarities of the underlying function  $\mathbf{f}$ . More precisely, we are interested in the solution flows  $\mathbf{x}_i(t) \in \mathbb{R}^n$  defined by the dynamical system

$$\dot{\mathbf{x}}_i := \pm \mathbf{u}_i(\mathbf{x}_i), \quad \mathbf{x}_i(0) = \widetilde{\mathbf{x}}, \tag{4}$$

or the corresponding solution flows  $\mathbf{y}_i(t) \in \mathbb{R}^m$ , defined by

$$\dot{\mathbf{y}}_i := \pm \sigma_i(\mathbf{x}_i)\mathbf{v}_i(\mathbf{x}_i), \quad \mathbf{y}_i(0) = f(\widetilde{\mathbf{x}}),$$
 (5)

where  $(\sigma_i, \mathbf{u}_i, \mathbf{v}_i)$  is the *i*th singular triplet of  $\mathbf{f}'(\mathbf{x}_i)$ . The scaling in (5) ensures the relationship

$$\mathbf{y}_i(t) = \mathbf{f}(\mathbf{x}_i(t)). \tag{6}$$

The sign  $\pm$  in defining the vector field is meant to select the direction, so as to avoid the discontinuity jump because singular vectors are unique up to a sign change. Suppose  $\dot{\mathbf{x}}(t) = \mathbf{u}(\mathbf{x}(t))$  and we define  $\mathbf{z}(t) := \mathbf{x}(-t)$ , then  $\dot{\mathbf{z}}(t) = -\mathbf{u}(\mathbf{z}(t))$ . Thus, we may assume that—without loss of generality—the direction of singular vectors has been predestined and that the time t can move either forward or backward.

It must be noted that any given point  $\tilde{\mathbf{x}}$  at which  $\mathbf{f}'(\tilde{\mathbf{x}})$  has at least one isolated singular vector cannot be an equilibrium point of the dynamical system (4). Therefore, the frame must move. What can happen is that the right side of (4) (or (5)) is not well-defined at points when singular values coalesce because at such points,  $\mathbf{f}'(\mathbf{x})$  has multiple singular vectors corresponding to the same singular value. A missed choice might cause  $\dot{\mathbf{x}}_i$  (or  $\dot{\mathbf{y}}_i$ ) to become discontinuous. We shall argue in this paper that it is precisely at these points that the nearby dynamics manifest significantly different behaviors. Such a discontinuity is not to be confused with the theory of analytic singular value decomposition (ASVD), which asserts the existence of an analytic factorization for an analytic function in  $\mathbf{x}$  [7,8]. The subtle difference is that the ASVD guarantees an analytic decomposition as a whole, but once we begin to pick out a specific singular vector, such as insisting that  $\mathbf{u}_1(\mathbf{x})$  always denotes the right singular vector associated with the largest singular value  $\sigma_1$ , then  $\mathbf{u}_1(\mathbf{x})$  by itself cannot guarantee its analyticity at the place where  $\sigma_1 = \sigma_2$ .

Because of how they are constructed, the integral curves  $\{x_i(t)\}$  and  $\{y_i(t)\}$  are referred to in this paper as the right and the left *singular curves* (The term "singular curve" has been used in a different context in the literature. See, for example, [9]. We emphasize its association with the singular value decomposition. Also, the notion of singular curves is fundamentally different from the notion of principal curves used in statistics [10–13]) of map f, respectively. It suffices to consider only the right singular curves because the relationship (6) implies that their images under f are precisely the left singular curves. What makes singular curves interesting is that they represent some curious undercurrents not recognized before the functions. Each function carries its own inherent flows. We conjecture that under appropriate conditions, a given set of trajectories should also characterize a function. Exactly how such a correspondence between singular curves and a function takes place remains an open question.

Singular value curves do exist for smooth functions over spaces of arbitrary dimensions. In this paper, we study only the singular curves for two-parameter functions so that we can actually visualize the dynamics. In particular, we focus on how it affects parametric surfaces in  $\mathbb{R}^3$ . Under this setting, it suffices to consider only the principal singular curves  $\mathbf{x}_1(t)$  because the secondary singular curves  $\mathbf{x}_2(t)$  are simply the orthogonal curves to  $\mathbf{x}_1(t)$ . Limiting ourselves to two-parameter functions seems to have overly simplified the task. However, we shall demonstrate that the corresponding dynamics already reveal some remarkably amazing exquisiteness.

The study of surfaces is a classic subject with a long history and rich literature, both theoretically and practically. Research endeavors range from abstract theory in pure mathematics [14–16] to the study of minimal surfaces [17,18] and applications in computer

Mathematics 2023, 11, 3306 4 of 20

graphics, security, and medical images [19–21]. For instance, perhaps the best-known classification theorem for surfaces is that any closed connected surface is homeomorphic to exactly one of the following surfaces: a sphere, a finite connected sum of tori, or a sphere with a finite number of disjoint discs removed (with cross-caps glued in their place) [22]. To extract fine grains of surfaces, more sophisticated means have been developed. For example, the classic conformal geometry approach uses discrete Riemann mapping and Ricci flow for parameterization, matching, tracking, and identification for surfaces with an arbitrary number of genera [20,23]. See also reference [24], where the Laplace–Beltrami spectra are used as isometric-invariant shape descriptors. We hasten to acknowledge that we do not have the expertise to elaborate substantially on these and other alternative methods for extracting geometric features of surfaces. We are not in a position to make a rigorous comparison. We simply want to mention that, while these approaches are plausible, they might encounter three challenges, i.e., the associated numerical algorithms are usually complicated and expensive; the techniques designed for one particular problem are often structure-dependent and might not be easily generalizable to another type of surface; and, most disappointingly, they cannot decipher what really causes a surface to behave in the way we expect it to behave. In contrast, our approach is at a much more basic level than most of the studies in the literature. We concentrate on the dynamics that govern the structural dissimilarity of every smooth surface.

This work, which uses the information-bearing singular value decomposition to study smooth nonlinear functions, revealing a fascinating undercurrent per the given function, is perhaps the first of its kind. Our goal in this presentation, therefore, is aimed at merely conveying the point that the dynamical system of singular vectors dictates how a smooth function varies and vice-versa. In particular, our initial investigation suggests that a surprising and universal structure that is remarkably analogous to the biological DNA formation, which is associated with a general parametric surface in  $\mathbb{R}^3$ , involves two strands of critical curves in  $\mathbb{R}^2$ , strung with a sequence of eight distinct base pairings whose folding and ordering might encode the behavior of a surface. Thus, a tantalizing new prospect emerges—would it be possible that a surface could be genome-sequenced and synthesized, and that its geometric properties could be explained by the makeup of genes? This new subject is far from understood. This work is only the first step in which we hope to stimulate some general interest.

This paper is organized as follows. For high-dimensional problems, it is not possible to characterize the vector field (4) explicitly. For two-parameter maps, we can describe the dynamical system in terms of two basic critical curves. These basics are outlined in Section 2. The intersection points of these critical curves are precisely where the dynamical system breaks down and, hence, contribute to the peculiar behavior of the system. In Section 3, we demonstrate the interesting behavior of the singular curves by considering several well-known parametric surfaces, such as the Klein bottle, the Boy face, the snail, and the breather surfaces. The first-order local analysis of the dynamical system is given in Section 4. By bringing in the second-order information in Section 5, we can further classify the local behavior in terms of base pairings, which provide a universal structure underneath all generic parametric surfaces. In Section 6, we recast the singular vector dynamics over the classical scalar-valued functions and give a précis of how the notion of base pairing should be modified into "wedges" for this simple case. Finally, in Section 7, we outline a few potential applications, including a comparison with gradient flows and a demonstration of the base pairing sequence.

#### 2. Basics

Given a differentiable two-parameter function  $f: \mathbb{R}^2 \to \mathbb{R}^m$ , we denote the two columns of its  $m \times 2$  Jacobian matrix by

$$\mathbf{f}'(\mathbf{x}) = [ \mathbf{a}_1(\mathbf{x}), \mathbf{a}_2(\mathbf{x}) ].$$

Mathematics 2023, 11, 3306 5 of 20

Define the two scalar functions

$$\begin{cases}
 n(\mathbf{x}) := \|\mathbf{a}_2(\mathbf{x})\|^2 - \|\mathbf{a}_1(\mathbf{x})\|^2, \\
 o(\mathbf{x}) := 2\mathbf{a}_1(\mathbf{x})^\top \mathbf{a}_2(\mathbf{x}),
\end{cases} (7)$$

that measure the disparity of norms and nearness of orthogonality between the column vectors of  $\mathbf{f}'(\mathbf{x})$ , respectively. Correspondingly, define the two sets:

$$\begin{cases}
\mathcal{N} := \{\mathbf{x} \in \mathbb{R}^n \mid n(\mathbf{x}) = 0\}, \\
\mathcal{O} := \{\mathbf{x} \in \mathbb{R}^n \mid o(\mathbf{x}) = 0\}.
\end{cases}$$
(8)

Generically, each set forms a one-dimensional manifold in  $\mathbb{R}^2$ , which is possibly empty or composed of multiple curves or loops. They will be shown in our analysis to play the role of "polynucleotide", connecting a string of interesting points and characterizing certain properties of a function.

A direct computation shows that the two singular values of f'(x) are given by

$$\begin{cases}
\sigma_{1}(\mathbf{x}) := \left(\frac{1}{2}\left(\|\mathbf{a}_{1}(\mathbf{x})\|^{2} + \|\mathbf{a}_{2}(\mathbf{x})\|^{2} + \sqrt{\sigma(\mathbf{x})^{2} + n(\mathbf{x})^{2}}\right)\right)^{1/2}, \\
\sigma_{2}(\mathbf{x}) := \left(\frac{1}{2}\left(\|\mathbf{a}_{1}(\mathbf{x})\|^{2} + \|\mathbf{a}_{2}(\mathbf{x})\|^{2} - \sqrt{\sigma(\mathbf{x})^{2} + n(\mathbf{x})^{2}}\right)\right)^{1/2}.
\end{cases} (9)$$

The corresponding right singular vectors (expressions for both  $\mathbf{u}_1$  and  $\mathbf{u}_2$ , are given, but we will carry out the analysis for  $\mathbf{x}_1(t)$  only as that for  $\mathbf{x}_2(t)$  can be done similarly. Also,  $\mathbf{x}_2(t)$  is simply the orthogonal curve of  $\mathbf{x}_1(t)$  in  $\mathbb{R}^2$ ) are:

$$\mathbf{u}_{1}(\mathbf{x}) := \frac{\pm 1}{\sqrt{1 + \omega(\mathbf{x})^{2}}} \begin{bmatrix} \omega(\mathbf{x}) \\ 1 \end{bmatrix}, \tag{10}$$

$$\mathbf{u}_{2}(\mathbf{x}) := \frac{\pm 1}{\sqrt{1 + \zeta(\mathbf{x})^{2}}} \begin{bmatrix} \zeta(\mathbf{x}) \\ 1 \end{bmatrix}, \tag{11}$$

respectively, where

$$\begin{cases}
\omega(\mathbf{x}) &:= \frac{o(\mathbf{x})}{n(\mathbf{x}) + \sqrt{o(\mathbf{x})^2 + n(\mathbf{x})^2}}, \\
\zeta(\mathbf{x}) &:= \frac{-n(\mathbf{x}) - \sqrt{o(\mathbf{x})^2 + n(\mathbf{x})^2}}{o(\mathbf{x})}.
\end{cases} (12)$$

In the above, we normalize the second entry of the singular vectors with the understanding of taking limits when either  $\omega(\mathbf{x})$  or  $\zeta(\mathbf{x})$  becomes infinity. The following fact is observed immediately from (10).

**Lemma 1.** The tangent vectors to the singular curves  $\mathbf{x}_1(t)$  at any points in  $\mathcal{N}$ , but not in  $\mathcal{O}$ , are always parallel to either  $\mathbf{\alpha}_n := \frac{1}{\sqrt{2}}[1, 1]^\top$  or  $\mathbf{\beta}_n := [1, -1]^\top$ , depending on whether  $o(\mathbf{x})$  is positive or negative. Likewise, the tangent vectors of the singular curves at any points in  $\mathcal{O}$ , but not in  $\mathcal{N}$ , are parallel to  $\mathbf{\alpha}_0 := [0, 1]^\top$  or  $\mathbf{\beta}_0 := [1, 0]^\top$ , depending on whether  $n(\mathbf{x})$  is positive or negative.

At places where  $\mathcal N$  and  $\mathcal O$  intersect, which will be called *singular points*, the singular values coalesce and the (right) singular vectors become ambiguous. We shall argue that the intersection angles by  $\mathcal N$  and  $\mathcal O$  at the singular points affect the intriguing dynamics. The one-dimensional manifolds,  $\mathcal N$  and  $\mathcal O$ , can be thought of as stringing singular points together (with particular pairings) and will be referred to as the *critical curves* of  $\mathbf f$ .

It might be best to plot the above basic curves with some curious graphic examples. Consider the various two-parameter maps defined in Table 1, each representing some peculiar features. Repeatedly applying a high-precision numerical ODE integrator

Mathematics 2023, 11, 3306 6 of 20

to the differential systems (4) from starting points at different locations in the window  $[-5,5] \times [-5,5]$ , we find its singular curves  $\mathbf{x}_1(t)$  behave like those in the drawing of Figure 1, whereas its critical curves are sketched in the drawing of Figure 2. By overlaying the corresponding drawings in Figures 1 and 2, we can catch a glimpse into how these critical curves affect the dynamics of singular curves. In particular, the singular curves  $\mathbf{x}_1(t)$  make interesting twists nearby, where  $\mathcal N$  and  $\mathcal O$  intersect. The analysis of the angles at which the critical curves cut across each other will be detailed in the sequel. To demonstrate our point, an enlarged drawing over a coarser grid for Example 1 is depicted in Figure 3. Note that there are regions where the critical curves are extremely close to each other, forming long and narrow ridges with  $\sigma_2/\sigma_1 > 0.95$ .

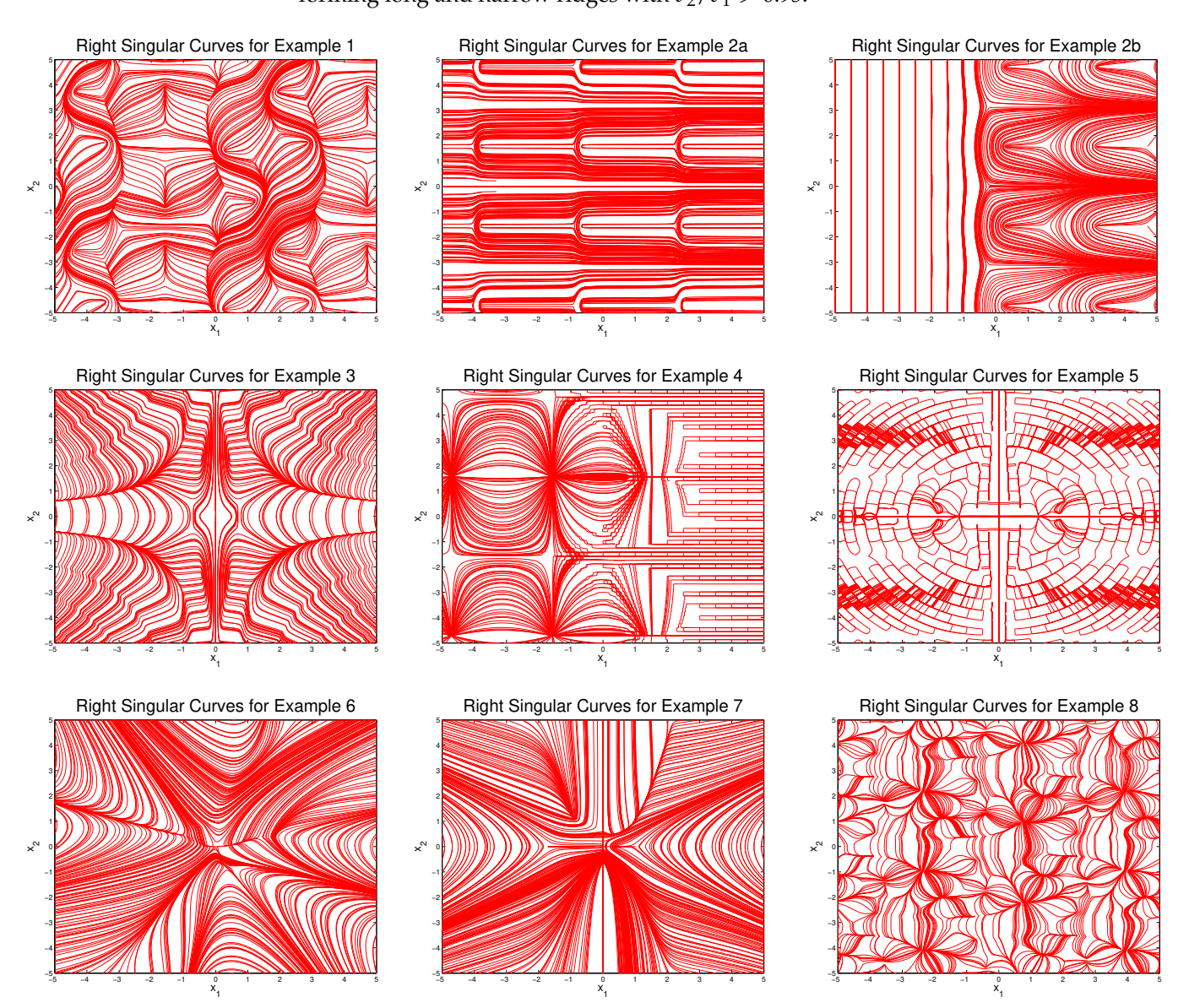


**Figure 1.** Examples of right singular curves  $\mathbf{x}_1(t)$ .

Mathematics **2023**, 11, 3306 7 of 20

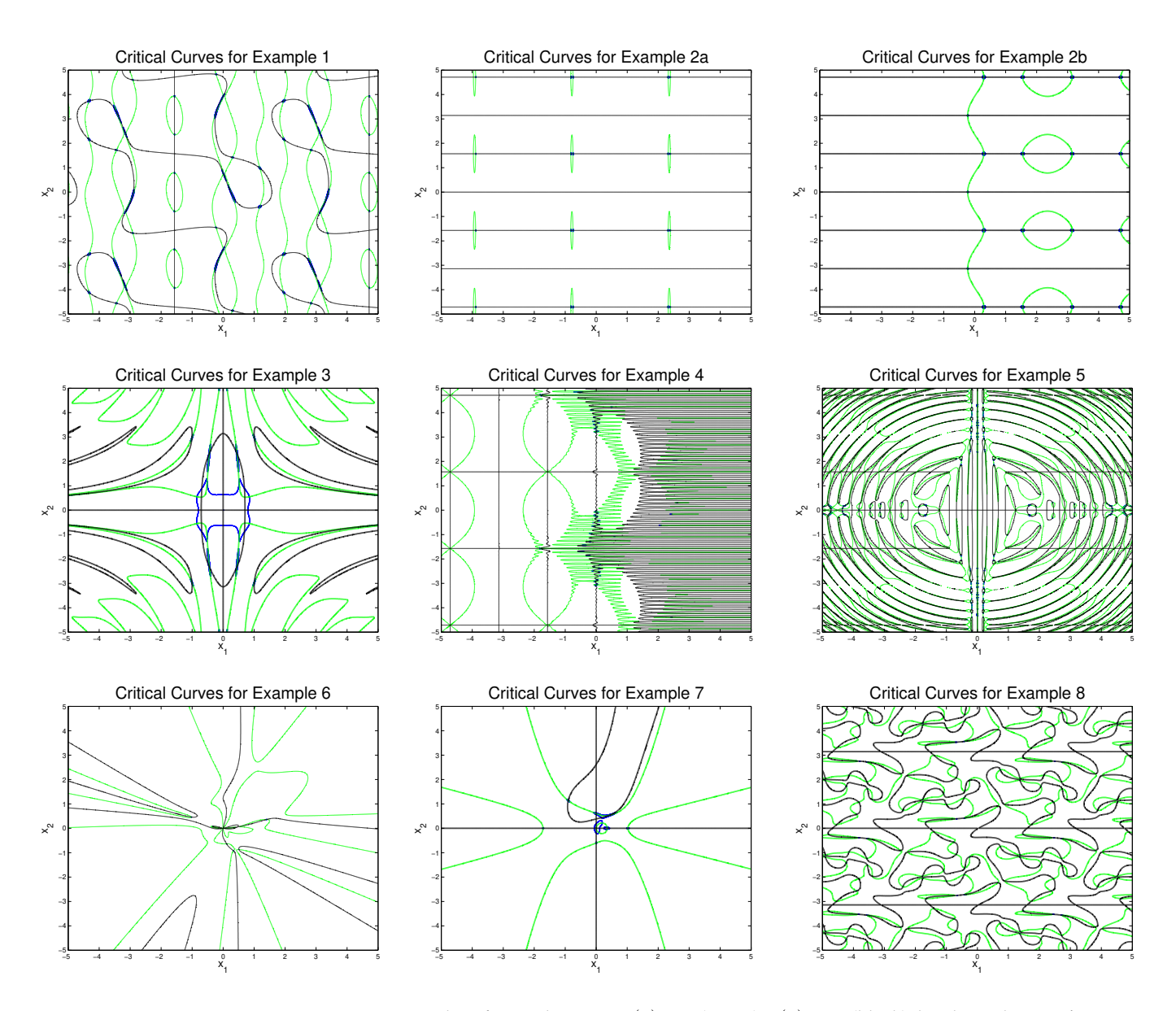


**Figure 2.** Examples of critical curves:  $n(\mathbf{x}) = 0$  (green);  $o(\mathbf{x}) = 0$ , (black); borders where  $\sigma_2/\sigma_1 \ge 0.95$ , (blue, not always shown if the region is too small).

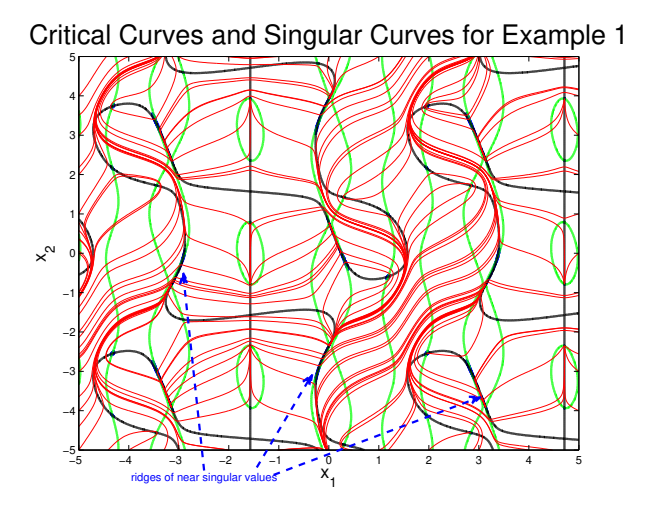


**Figure 3.** Superposition of singular curves and critical curves for example 1:  $n(\mathbf{x}) = 0$  (green);  $o(\mathbf{x}) = 0$ , (black); singular curves (red); ridges of near singular values (pointed by blue arrows).

Mathematics 2023, 11, 3306 8 of 20

<b>Table 1.</b> List of sample fur	nctions.
------------------------------------	----------

Example 1	Example 2a	Example 2b
$\begin{bmatrix} \sin(x_1 + x_2) + \cos(x_2) - 1 \\ \cos(2x_1) + \sin(x_2) - 1 \end{bmatrix}$	$\left[\begin{array}{c} e^{x_1}\cos(x_2) \\ 20e^{x_1}\sin(x_1) \end{array}\right]$	$\begin{bmatrix} e^{x_1}\cos(x_2) \\ e^{x_1}\sin(x_1) \\ x_2 \end{bmatrix}$
Example 3	Example 4	Example 5
$\begin{bmatrix} 4 + x_1 \cos(x_2/2) \\ x_2 \\ x_1 \sin(x_1 x_2/2) \end{bmatrix}$	$\begin{bmatrix} e^{x_1}\cos(20x_2) \\ 20e^{\sin(x_2)}\sin(x_1) \end{bmatrix}$	$\begin{bmatrix} \sin(x_1^2 + x_2^2)\cos(x_2) \\ 2e^{-2x_2^2x_1^2}\cos(10\sin(x_1)) \end{bmatrix}$
Example 6 [25]	Example 7	Example 8 [26]
$\begin{bmatrix} \begin{pmatrix} -270x_1^4x_2^3 - 314x_1x_2^4 \\ -689x_1x_2^3 + 1428 \end{pmatrix} \\ 36x_1^7 + 417x_1^6x_2 \\ -422x_1^5x_2^2 - 270x_1^4x_2^3 \\ +1428x_1^3x_2^4 - 1475x_1^2x_2^5 \\ +510x_1x_2^6 - 200x_1^6 \\ -174x_1^5x_2 - 966x_1^4x_2^2 \\ +529x_1^3x_2^3 + 269x_1^2x_2^4 \\ +49x_1x_2^5 - 267x_2^6 \\ +529x_1^4x_2 + 1303x_1^2x_2^3 \\ -314x_1x_2^4 + 262x_2^5 \\ +36x_1^4 - 788x_1^2x_2^2 \\ -689x_1x_2^3 + 177x_2^4 \end{bmatrix}$	$\begin{bmatrix} x_1 - \frac{x_1^2}{3} + x_1 x_2^2 \\ x_2 - \frac{x_2^3}{6} + x_2 x_1^3 \\ x_1^2 - x_2^3 \end{bmatrix}$	$\begin{bmatrix} \begin{pmatrix} \frac{1}{2}(2\rho^{2} - \phi^{2} - \psi^{2}) \\ +2\phi\psi(\phi^{2} - \psi^{2}) \\ +\psi\rho(\rho^{2} - \psi^{2}) \\ +\rho\phi(\phi^{2} - \rho^{2})) \end{pmatrix} \\ \begin{pmatrix} \frac{\sqrt{3}}{2}(\phi^{2} - \psi^{2} \\ +(\psi\rho(\psi^{2} - \rho^{2}) \\ +\rho\phi(\phi^{2} - \rho^{2}))) \end{pmatrix} \\ \begin{pmatrix} (\rho + \phi + \psi) \\ *((\rho + \phi + \psi)^{3} \\ +4(\phi - \rho)(\psi - \phi) \\ *(\rho - \psi)) \end{pmatrix}$ with $\begin{cases} \rho = \cos(x_{1})\sin(x_{2}) \\ \phi = \sin(x_{1})\sin(x_{2}) \\ \psi = \cos(x_{2}) \end{cases}$

## 3. Application to Parametric Surfaces

In this section, we apply the notion of singular curves to a few renowned but more complicated 3D surfaces to further demonstrate the associated critical curves, singular points, and the trajectories of (left) singular curves on the surfaces (Admittedly, it is difficult to render a satisfactory 3D drawing unless one can view the surface from different perspectives. The singular curves presented here are simply some snapshots of the far more complicated dynamics. We can furnish our beta version software for readers to interactively play out the evolution of the singular curve at arbitrarily selected locations in  $\mathbb{R}^2$ . A mechanism that can perform local analysis was also built into our code, as we shall explain in the next section). In all cases, we denote the two-parameter map in the form  $\mathbf{f}(x_1, x_2) = (X(x_1, x_2), Y(x_1, x_2), Z(x_1, x_2))$ , whose components are abbreviated as (X, Y, Z). Our point is that the surfaces might be complicated in  $\mathbb{R}^3$ , but the dynamics of the (right) singular curves could be surprisingly simple in  $\mathbb{R}^2$ . The shapes of the critical curves and the sequences of the base pairings together seem sufficient to characterize a particular surface.

**Example 9:** (Klein bottle). The well-known Klein bottle can be characterized by the following parametric equations:

$$\begin{cases} X := -\frac{2}{15}c_1(3c_2 + 5s_1c_2c_1 - 30s_1 - 60s_1c_1^6 + 90s_1c_1^4), \\ Y := -\frac{1}{15}s_1(80c_2c_1^7s_1 + 48c_2c_1^6 - 80c_2c_1^5s_1 - 48c_2c_1^4 - 5c_2c_1^3s_1 - 3c_2c_1^2 + 5s_1c_2c_1 + 3c_2 - 60s_1), \\ Z := \frac{2}{15}s_2(3 + 5s_1c_1), \end{cases}$$

where the parameters  $x_1 \in [-\pi, \pi]$  and  $x_2 \in [-\pi, \pi]$  are embedded in  $c_1 := \cos x_1$ ,  $s_1 := \sin x_1$ ,  $c_2 := \cos x_2$ , and  $s_2 := \sin x_2$ . In the left drawing of Figure 4, we find that critical curves for this particular Klein bottle are surprisingly simple. There is no  $\mathcal{N}$  curve at all, whereas the  $\mathcal{O}$  curves form vertical and horizontal grids. Therefore, there is no singular point in this case. We sketch two (right) singular curves by integrating the

Mathematics 2023, 11, 3306 9 of 20

dynamics system (4) in both forward (red) and backward (blue) times from two distinct start points (the forward and backward directions of integration are relative to the singular vector chosen at the starting point  $\tilde{\mathbf{x}}$ . Such a distinction is really immaterial. We mark them differently only to identify the starting point. If, however, the vector field  $\mathbf{u}_1(\mathbf{x})$  is obtained through numerical calculations, then we must be aware that a general-purpose SVD solver cannot guarantee the continuity of  $\mathbf{u}_1(\mathbf{x}(t))$ , even if  $\mathbf{x}(t)$  is continuous in t. An additional mechanism must be made to ensure that  $\mathbf{u}_1(\mathbf{x}(t))$  does not abruptly reverse its direction, once the initial direction is set), which are identifiable at the places where the colors are changed. It is interesting to note that, in this example, all right singular curves are horizontal, whereas their images, namely, the corresponding left singular curves, are periodic on the bottle, and wind the bottle twice. To manifest the dynamics of the left singular curves on the Klein bottle, we remove the surface and draw only the 3D curves in the right drawing of Figure 4.

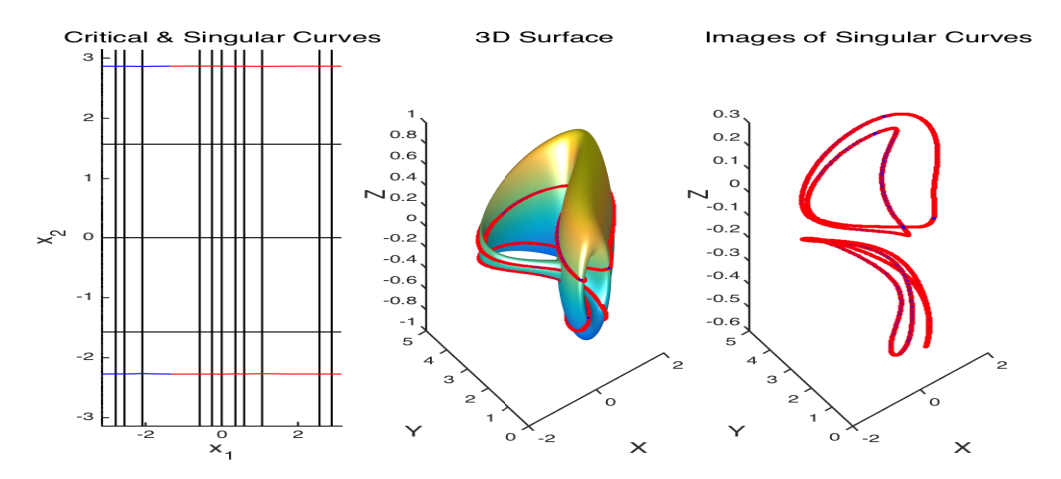


**Figure 4.** Klein bottle:  $\mathcal{N}$  (green);  $\mathcal{O}$  (black); left singular curves (forward time (red); backward time (blue, overwritten)).

If we perturb the equation by modifying some coefficients, the resulting surface is topologically equivalent to the original bottle. However, the critical curves are very different. The drawing in Figure 5 is the flattened bottle, where the Y component is scaled down to 10% of its original value, i.e., the coefficient  $-\frac{1}{15}$  is changed to  $-\frac{1}{150}$ . Note that now there are  $\mathcal N$  curves and singular points and that the left singular curves are no longer periodic. This kind of distinction is significant because it shows the idiosyncrasies even among topologically equivalent surfaces.

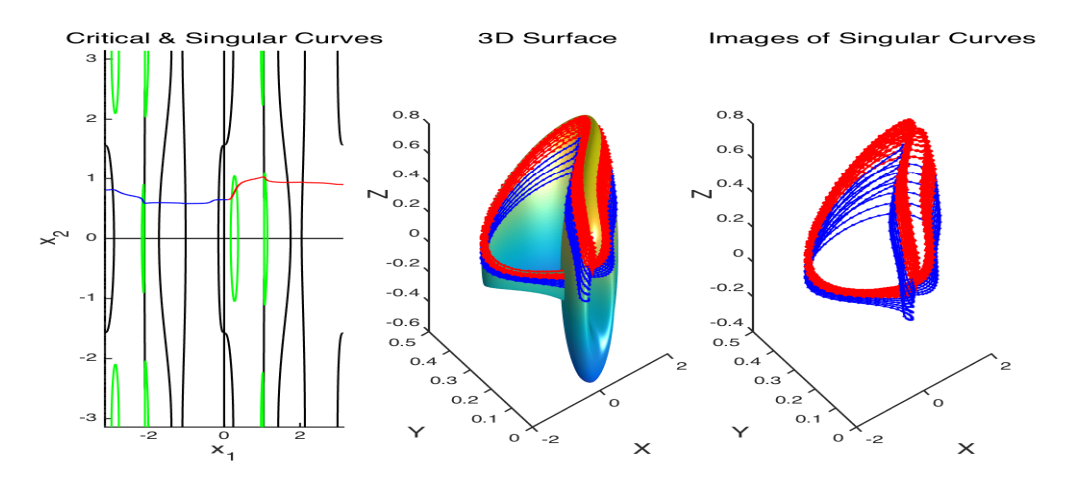


**Figure 5.** Klein bottle with Y downscaled:  $\mathcal{N}$  (green);  $\mathcal{O}$  (black); singular curves (forward time (red); backward time (blue)).

Mathematics 2023, 11, 3306 10 of 20

**Example 10.** (Boy's surface). For parameters  $x_1 \in [0, \pi]$  and  $x_2 \in [0, 2\pi]$ , define  $p := \cos x_1 \sin x_2$ ,  $q := \sin x_1 \sin x_2$ , and  $r := \cos x_2$ . Then the famous non-orientable Boy's surface can be described analytically by the parametric equations [26]:

$$\left\{ \begin{array}{ll} X & :=: & (2p^2-q^2-r^2+2qr(q^2-r^2)+rp(p^2-r^2)+pq(q^2-p^2)), \\ Y & := & \frac{\sqrt{3}}{2}(q^2-r^2+(rp(r^2-p^2)+pq(q^2-p^2))), \\ Z & := & (p+q+r)((p+q+r)^3+4(q-p)(r-q)(p-r)). \end{array} \right.$$

As shown in the left drawing of Figure 6, the critical curves repeat themselves as jigsaw puzzles with periods  $\pi$  in both  $x_1$  and  $x_2$  directions, and there are many singular points in this case. We integrate one right singular curve, starting at the location (1,4.5) over the extended domain in the  $x_2$  direction to show how far it can migrate. A total of four singular points are involved. Going southwest, the forward time (red) integration passes by (but never touches) the first singular point A. Then, it makes a U-turn around a second singular point B and comes to a stop (due to the discontinuity) at a third singular point C. The backward time (blue) integration moves northeast, makes a U-turn around a fourth singular point D before it stops at the first singular point D. It is interesting to note that the first point D serves both as a roundabout and an attractor and that the fourth singular point D is a translation by D of the second singular point D. We rotate the D of the second singular point D is a translation by D of the second singular point D is a translation by D of the second singular point D is a translation by D of the second singular point D is a translation by D of the second singular point D is a translation by D of the second singular point D is a translation by D of the second singular point D is a translation by D of the second singular point D is a translation by D of the second singular point D is a translation by D of the second singular point D is a translation by D of the second singular point D is a translation by D of the second singular point D is a translation by D of the second singular point D is a translation of the second singular point D is a translation of the second singular point D is a translation of the second singular point D is a translation of the second singular point D is a translation of the second singular point D is a translation of the second singular point D is a translatio

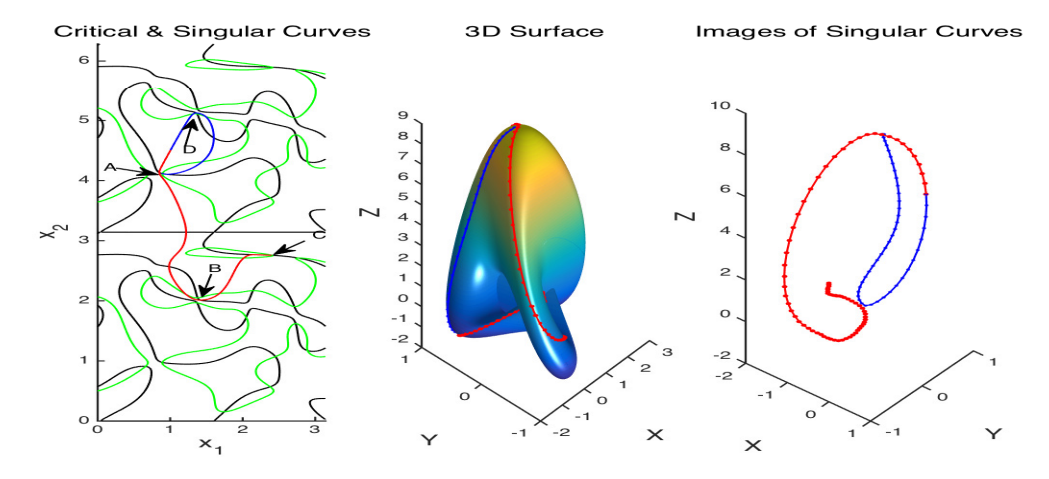


**Figure 6.** Boy's surface:  $\mathcal{N}$  (green);  $\mathcal{O}$  (black); singular curves (forward time (red); backward time (blue)).

**Example 11.** (Snail). It is interesting to note that, with  $v := x_2 + \frac{(x_2 - 2)^2}{16}$ ,  $s := e^{-\frac{1}{10v}}$ , and  $r := s + \frac{7}{5}s\cos x_1$  for the parameters  $x_1 \in [0, 2\pi]$  and  $x_2 \in [-10, 35]$ , points specified by the parametric equations are as follows:

$$\begin{cases} X := r \cos v, \\ Y := 4(1-s) + \frac{7}{5}s \sin x_1, \\ Z := r \sin v, \end{cases}$$

form a snail shape surface in  $\mathbb{R}^3$ . Despite the impression that the snail surface appears complicated, its critical curves are surprisingly simple. The left drawing in Figure 7 shows the  $\mathcal{O}$  curves are straight lines intersecting the  $\mathcal{N}$  curve at only two singular points in the given window. The mirror image of the  $\mathcal{N}$  curve, with respect to the horizontal  $\mathcal{O}$  curve, which produces exactly the same dynamics, is not shown. In the left drawing of Figure 7,

Mathematics 2023, 11, 3306 11 of 20

we integrate the right singular curve  $\mathbf{x}_1(t)$  from one particular starting point (where colors change). The forward (red) integration approaches asymptotically to the vertical  $\mathcal{O}$  curve. The corresponding left singular curve converges to the tip of the snail. The backward (blue) integration converges to a singular point, which indicates an "isotropic point" on the surface at which rates of change are identical in all directions. The snail does have a core inside the shell. The left singular curve plotted in the right drawing of Figure 7 traces that core.

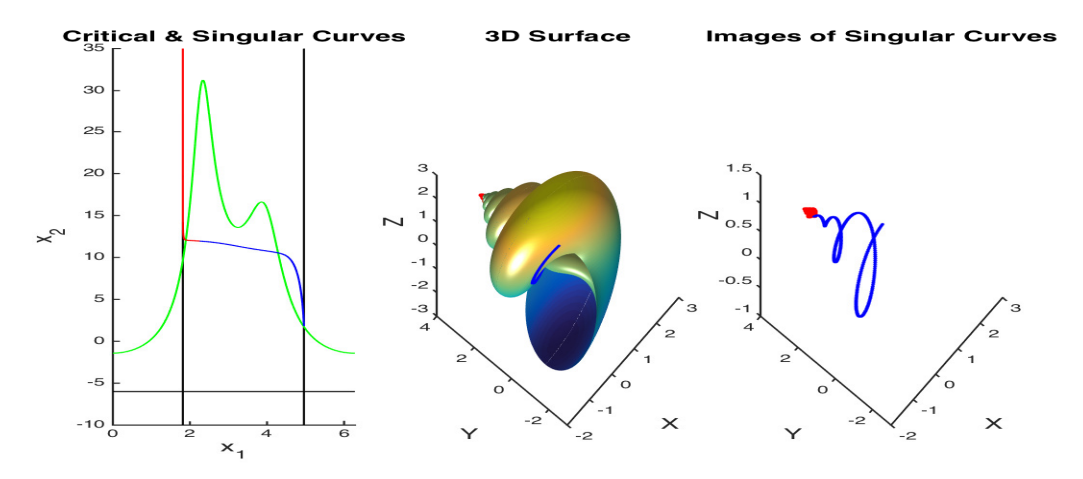


**Figure 7.** Snail:  $\mathcal{N}$  (green);  $\mathcal{O}$  (black); singular curves (forward time (red); backward time (blue)).

In Figure 8, we cut open the snail by restricting  $x_2 \in [-3,3]$  to demonstrates another singular curve starting from (2,-2). Note that its backward (blue) integration stays on the outside shell and converges to the tip of the snail, while its forward (red) integration loops around the opening mouth of the snail.

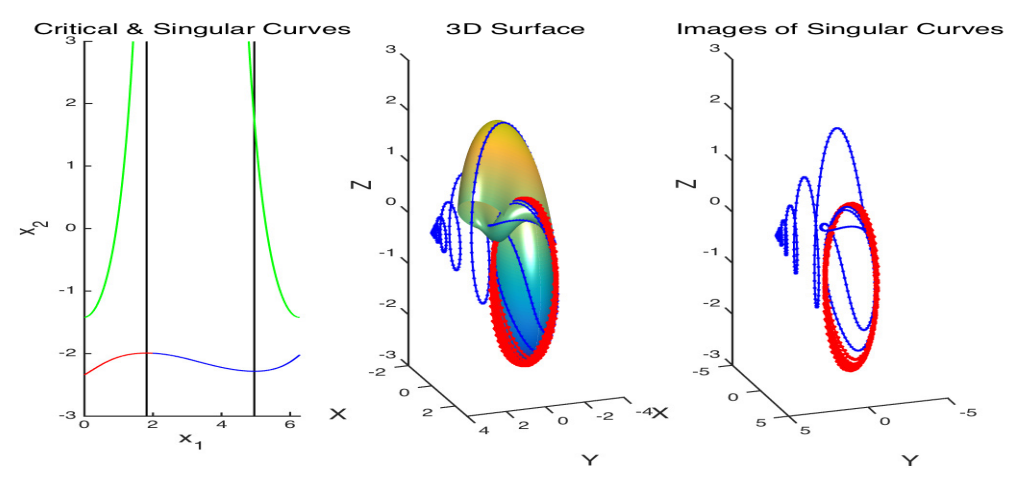


**Figure 8.** Opened snail:  $\mathcal{N}$  (green);  $\mathcal{O}$  (black); singular curves (forward time (red); backward time (blue)).

**Example 12.** (Breather). The breather surface is a generalized pseudo-sphere, which has special meaning in theoretical physics. Denote  $w:=\frac{\sqrt{21}}{5}$  and  $\rho:=\frac{2}{5}((w\cosh(\frac{2}{5}x_1))^2+(\frac{2}{5}\sin(wx_2))^2)$ . Then, one way to parameterize the breather surface is via the following equations:

$$\begin{cases} X := -x_1 + \frac{2w^2}{\rho} \cosh(\frac{2}{5}x_1) \sin(\frac{2}{5}x_1), \\ Y := \frac{2w \cosh(\frac{2}{5}x_1)}{\rho} (-w \cos(x_2) \cos(wx_2) - \sin(x_2) \sin(wx_2)), \\ Z := \frac{2w \cosh(\frac{2}{5}x_1)}{\rho} (-w \sin(x_2) \cos(wx_2) + \cos(x_2) \sin(wx_2)), \end{cases}$$

Mathematics 2023, 11, 3306 12 of 20

where  $x_1$  controls how far the tips extend outward and  $x_2$  controls how far the girth goes around. Starting with 0, every increment of  $x_2$  by  $\frac{5}{2\sqrt{21}}\pi\approx 3.42776$  defines one "vertebra" with two layers of "patagium" extended to the tips for a total of 22 vertebrae around the girth. We plot a portion of the surface with  $x_1\in [-5,5]$  and  $x_2\in [-2,5]$  and some singular curves in Figure 9. There are periodic left singular curves on the vertebra, so the color distinction of the trajectories becomes futile. The horizontal  $\mathcal O$  curves at  $x_2=0$ ,  $\frac{5}{2\sqrt{21}}\pi$ , and so on, are invariant under the right singular curve dynamics (4), whose corresponding left singular curves are precisely those "ribs" on the breather surface. Again, we find it interesting that critical curves and singular curves are simple when compared to the entirety of the breather surface.

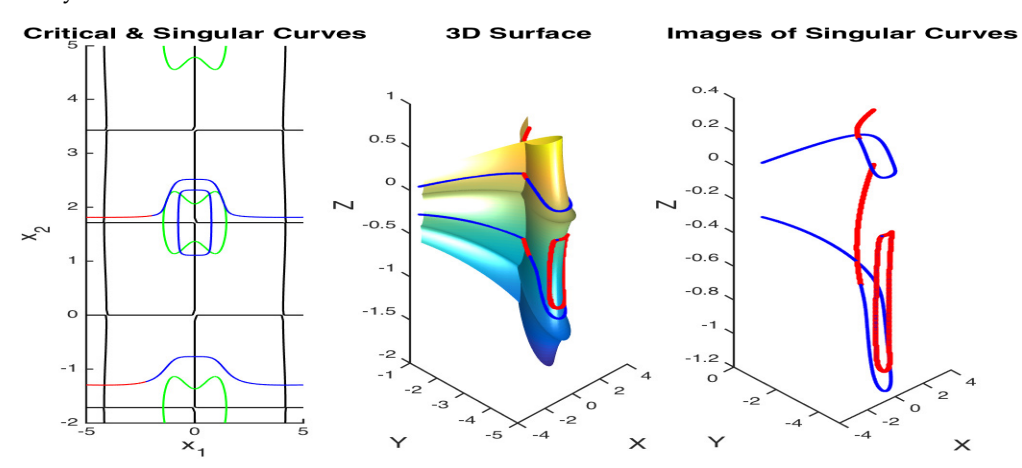


**Figure 9.** Breather:  $\mathcal{N}$  (green);  $\mathcal{O}$  (black); singular curves (forward time (red); backward time (blue)).

## 4. Local Behavior

Given the above illustrations, one big question is to understand what is going on behind these intriguing curves. In order to answer this question, we rewrite the dynamical system governing the (right) singular curves, as

$$\dot{\mathbf{x}} = \pm \frac{1}{\sqrt{2\sqrt{n(\mathbf{x})^2 + o(\mathbf{x})^2}}} \begin{bmatrix} \frac{o(\mathbf{x})}{\sqrt{n(\mathbf{x}) + \sqrt{n(\mathbf{x})^2 + o(\mathbf{x})^2}}} \\ \sqrt{n(\mathbf{x}) + \sqrt{n(\mathbf{x})^2 + o(\mathbf{x})^2}} \end{bmatrix}, \tag{13}$$

which clearly shows that there are no equilibrium points, but they become undefined at singular points. Let  $x_0$  be an isolated singular point. We now investigate the dynamical behavior nearby  $x_0$ .

Consider the scenario where  $\mathcal N$  and  $\mathcal O$  intersect in the scheme depicted in Figure 10. The short red segments denote tangent vectors of singular curves crossing the critical curves (here, we assume a generic case, where only one  $\mathcal N$  curve and one  $\mathcal O$  curve intersect at  $\mathbf x_0$ . It is possible that more than two critical curves are intersecting at a singular point, e.g., the monkey saddle. To present the basic idea, we consider only the generic case here) that take into account the signs of  $o(\mathbf x)$  and  $n(\mathbf x)$ . By Lemma 1, these directions are invariant on each half of the critical curves. The portions of  $\mathcal N$  and  $\mathcal O$ , where the tangent vectors of the crossing singular curves are parallel to the unit vectors  $\mathbf x_n = \frac{1}{\sqrt{2}}[1,1]^{\top}$  and  $\mathbf x_0 := [0,1]^{\top}$ , respectively, are referred to as the  $\mathbf x$  halves of the critical curves and denoted by  $\mathbf x$  and  $\mathbf x$ . Likewise, by changing  $\mathbf x$  to  $\mathbf x$ , we refer to the other halves of the critical curves. It is convenient to flag the critical curves with arrows to indicate the sides of  $\mathbf x$  and  $\mathbf x$ . In this generic case, the neighborhood of  $\mathbf x$ 0 is naturally divided into "quadrants" distinguished by the signs  $(\mathrm{sgn}(n(\mathbf x)), \mathrm{sgn}(o(\mathbf x)), \mathrm{which}$ , in a sense, imply a specific "orientation" of a local curvilinear coordinate system. With tangent vectors depicted in the left drawing of Figure 10, the flow of the singular curves near  $\mathbf x$ 0 should move away from  $\mathbf x$ 0, as is depicted

Mathematics 2023, 11, 3306 13 of 20

in the right diagram. In other words, the singular point  $\mathbf{x}_0$  acts like a repeller for the flows  $\mathbf{x}_1(t)$ . If the orientation is switched, such as that depicted in Figure 11, then the nearby dynamical behavior may change its topology.

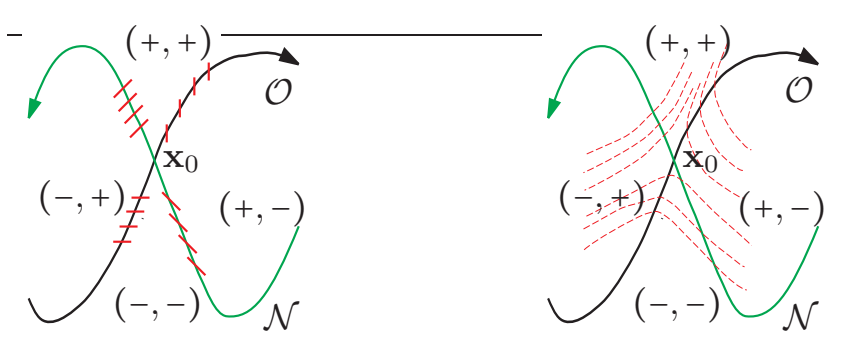


**Figure 10.** Local behavior near a propellant singular point  $x_0$ .

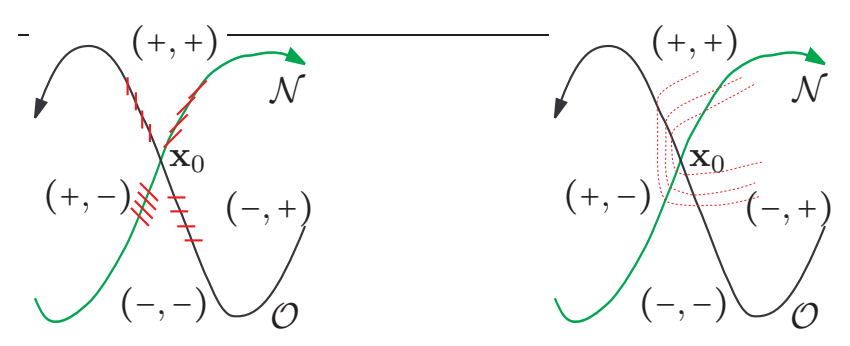


**Figure 11.** Local behavior near a roundabout singular point  $x_0$ .

The manifolds  $\mathcal{N}$  and  $\mathcal{O}$  near  $\mathbf{x}_0$  can be infinitesimally represented by their respective tangent vectors  $\boldsymbol{\tau}_n$  and  $\boldsymbol{\tau}_o$  at  $\mathbf{x}_0$ . Again, we flag the originally undirected vectors  $\boldsymbol{\tau}_n$  and  $\boldsymbol{\tau}_o$  with arrows pointing to the corresponding  $\alpha$  halves of the critical curves. Starting with the north, and centered at  $\mathbf{x}_0$ , we divide the plane into eight sectors, each with a central angle  $\frac{\pi}{4}$ , and assign an ordinal number to name the sectors clockwise. The relative positions of the two  $\alpha$  halves  $n_{\alpha}$  and  $o_{\alpha}$ , with respect to these sectors, are critical in deciding the local behavior. For easy reference, we say that we have configuration (i,j) when  $\boldsymbol{\tau}_n$  and  $\boldsymbol{\tau}_o$  are located in the i-th and the j-th sectors, respectively. There are a total of 64 possible configurations.

First consider the general case when  $\tau_n$  is not parallel to  $\alpha_n$  and  $\tau_o$  is not parallel to  $\alpha_o$ . Special cases can be discussed in a similar manner. As already demonstrated earlier in Figures 10 and 11, the orientations of  $\tau_n$  and  $\tau_o$  do matter. The 48 configurations (where  $i \neq j$  and  $|i-j| \neq 4$ ) already include  $\tau_n$  and  $\tau_o$  in reverse positions. Each of the eight configurations where i=j contains two distinct cases, when the orientations of  $\tau_n$  and  $\tau_o$  are swapped. Likewise, each of the eight configurations where |i-j|=4 also contains two distinct orientations. Using the ideas described in Figures 10 and 11 to conduct an exhaustive search, we sketch all 80 possible local behaviors in Figure 12, some of which are identical by rotations. Upon inspecting all the possibilities, we summarize our observations in the following lemma.

**Lemma 2.** Assume that a given singular point is the intersection of exactly one  $\mathcal{N}$  curve and one  $\mathcal{O}$  curve in its neighborhood. Assume also that at this point  $\tau_n$  is not parallel to  $\alpha_n$  and  $\tau_0$  is not parallel to  $\alpha_0$ . Then, the singular point serves to affect three essentially different dynamics, i.e., propellant, roundabout, or one-sided roundabout and one-sided attractor or propellant.

The local bearings are identified by the two-letter marks, namely, the pairings at the upper left corner in each case, which will be explained in the next section. We mention in

Mathematics 2023, 11, 3306 14 of 20

passing that every even-numbered column in the upper table in Figure 12 has the same paring as that in the odd column to its left.

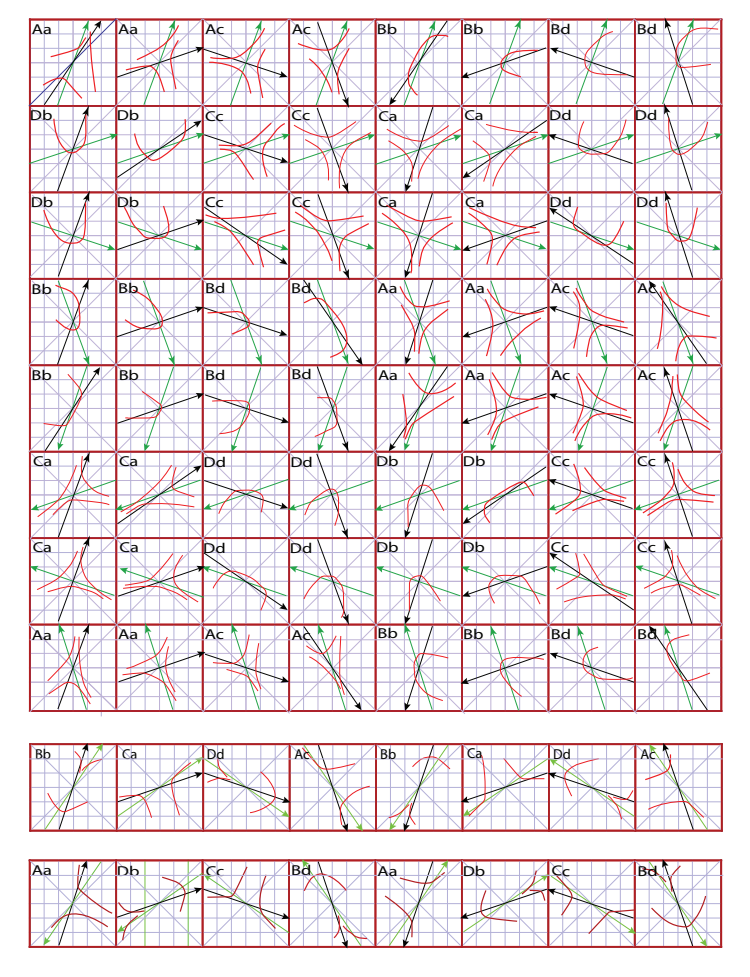


**Figure 12.** Eighty possible local behaviors near a singular point  $\mathbf{x}_0$ . Arrows point at the  $\alpha$  halves  $n_{\alpha}$  (green) and  $o_{\alpha}$  (black).

## 5. Base Pairing

To justify the various curling behaviors of  $\mathbf{x}_1(t)$  shown in Figure 12, we need to take into account more than just the first-order derivative  $\mathbf{u}_1(t)$ . Observe that  $\omega(\mathbf{x})$  can be expressed as

$$\omega(\mathbf{x}) := \begin{cases} sgn(o(\mathbf{x})) - \frac{n(\mathbf{x})}{o(\mathbf{x})} + \frac{sgn(o(\mathbf{x}))n(\mathbf{x})^{2}}{2o(\mathbf{x})^{2}} + O(n(\mathbf{x})^{3}), & near \ n(\mathbf{x}) = 0, \\ \frac{o(\mathbf{x})}{2n(\mathbf{x})} - \frac{o(\mathbf{x})^{3}}{8n(\mathbf{x})^{3}} + \frac{o(\mathbf{x})^{5}}{16n(\mathbf{x})^{5}} + O(o(\mathbf{x})^{7}), & near \ o(\mathbf{x}) = 0 \ and \ if \ n(\mathbf{x}) > 0, \\ \frac{o(\mathbf{x})}{2n(\mathbf{x})} - \frac{o(\mathbf{x})^{3}}{8n(\mathbf{x})^{3}} + \frac{o(\mathbf{x})^{5}}{16n(\mathbf{x})^{5}} + O(o(\mathbf{x})^{7})', & near \ o(\mathbf{x}) = 0 \ and \ if \ n(\mathbf{x}) < 0. \end{cases}$$
(14)

We already know that the first derivative of  $\mathbf{x}_1(t)$  is related to  $\omega(\mathbf{x}_1(t))$  via (10). The expansion (14) of  $\omega(\mathbf{x})$  can now be used to estimate the second derivative of  $\mathbf{x}_1(t)$ . In this way, we can characterize the concavity property and the local behaviors observed in Figure 12.

As an example, consider the case that we are at a point on  $n_{\alpha}$ , where the singular flow necessarily points in the direction  $\alpha_n$ . Then, it follows from (14) that the value of  $\omega(\mathbf{x}(t))$  will increase if the vector  $\mathbf{x}(t)$  moves to the side, where  $n(\mathbf{x}) < 0$ , implying that the slope of the tangent vector  $\mathbf{u}_1(\mathbf{x}(t))$  must be less than 1. Likewise, if  $\mathbf{x}(t)$  moves to the side where  $n(\mathbf{x}) > 0$ , then the slope of  $\mathbf{u}_1(\mathbf{x}(t))$  must be greater than 1. We, therefore, know how  $\mathbf{x}(t)$  is bent.

Mathematics 2023, 11, 3306 15 of 20

A careful analysis concludes that, in all, near a singular point  $\mathbf{x}_0$  and relative to a fixed  $\tau_n$ , there are only four basic patterns, marked as A, B, C, and D, where the singular curves can cross the critical curve  $\mathcal{N}$ . Noting that  $\tau_n$  can be rotated to the points in other directions, we sketch a few possible concavities of  $\mathbf{x}_1(t)$  in Figure 13.

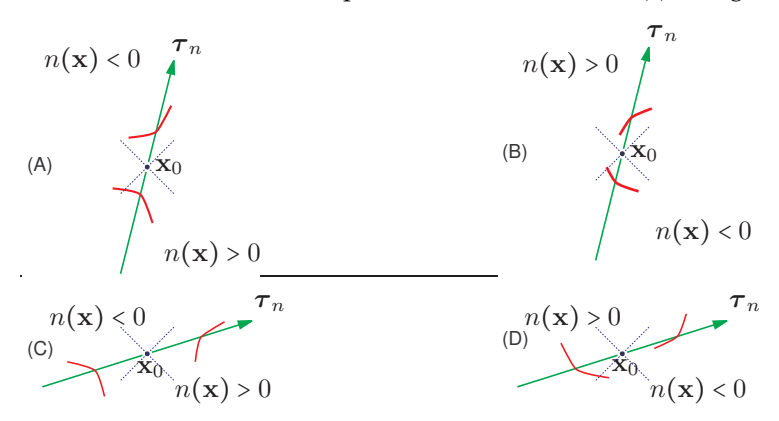


**Figure 13.** Basic concavities of singular curves near  $n(\mathbf{x}) = 0$ .

Similarly, suppose that we are at a point on  $o_\alpha$ , where the singular flow necessarily points in the direction of  $\alpha_0$ . If the vector  $\mathbf{x}(t)$  veers to the side where  $\frac{o(\mathbf{x})}{n(\mathbf{x})} > 0$ , then  $\omega(\mathbf{x})$  increases from 0 and, hence, the absolute value of the slope of the tangent vector  $\mathbf{u}_1(\mathbf{x}(t))$  must decrease, causing the bend. Again, there are four basic concavities of  $\mathbf{x}_1(t)$ , marked as  $\mathbf{a}$ ,  $\mathbf{b}$ ,  $\mathbf{c}$ , and  $\mathbf{d}$ , near  $\mathcal{O}$ , subject to rotations, as depicted in Figure 14.

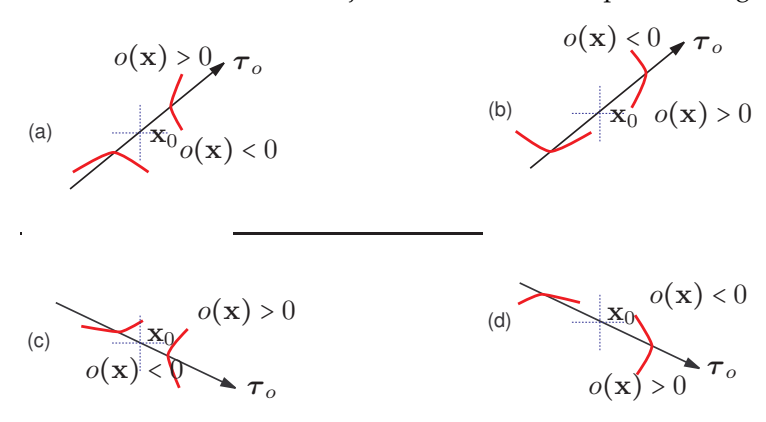


**Figure 14.** Basic concavities of singular curves near  $o(\mathbf{x}) = 0$ .

Paring the second-order derivative information along both the  $\mathcal N$  curve and the  $\mathcal O$  curve does not give rise to 16 cases. Instead, after carefully examining the 80 possible dynamics in Figure 12, we make the following interesting observation.

**Theorem 1.** Assume that a given singular point is the intersection of exactly one  $\mathcal{N}$  curve and one  $\mathcal{O}$  curve in its neighborhood. Assume also that, at this point,  $\tau_n$  is not parallel to  $\alpha_n$  and  $\tau_0$  is not parallel to  $\alpha_0$ . Then, the local behavior of the singular curves can be one of eight possible patterns identified by the base parings Aa, Ac, Bb, Bd, Ca, Cc, Db, and Dd only. There is no other possible combination.

**Proof.** The result is from a direct comparison, case-by-case. More specifically, we have four ways of describing the concavity along the  $\mathcal N$  curve near a singular point  $\mathbf x_0$ . These are cases (A) and (C), where  $\mathbf x_0$  behaves like a propellant, and cases (B) and (D), where  $\mathbf x_0$  behaves like a roundabout. In the meantime, we have four similar ways of describing the concavity along the  $\mathcal O$  curve. Under the assumption, case (A) or (C) can pair with (a) or (c) only to obtain a propellant. A pairing of Ab or Ad is not possible because it will require the singular curve near  $\mathbf x_0$  to have both a positive tangent and a negative

Mathematics 2023. 11, 3306 16 of 20

tangent simultaneously. Likewise, case (B) or (D) can pair with (b) or (d) only, whence  $\mathbf{x}_0$  serves as either a roundabout or a mixture of a one-sided roundabout and one-sided repeller/attractor.  $\square$ 

Each drawing in Figure 12 is identified by two letters of base parings in the upper left corner to indicate the corresponding dynamics. Each base paring has its own characteristic traits, which can be distinguished by visualization, e.g., the difference between both Aa and Ac in configurations (1,2) and (1,3) are repellers, according to whether the tailing is above or below  $\beta_o$ . We shall not categorize the details as they might be too tedious to describe in this paper. It is the combined effects of these basic curvatures that we refer to as base pairings, together with the positions of  $\tau_n$  and  $\tau_o$ , which makes up the local dynamics observed in Figure 12. It is worth noting that a quick count shows that each base pairing results in eight dynamics in the top drawing as general cases and two in the middle or bottom drawings as special cases. In Section 6, we shall characterize another situation where different types of pairings might occur.

In the examples outlined in Section 3, there are cases that are not covered in Figure 12. Still, local behaviors of singular curves can be analyzed similarly, but need more details. One aspect is that they depend not only on the relative positions of the tangent vectors  $\tau_0$  to  $\tau_n$  but also on which side of  $\tau_n$  that the  $\alpha$ -half  $n_\alpha$  resides. For instance, consider the scenario depicted in Figure 15, where  $\tau_n$  points to the northeast and  $\tau_0$  is neither parallel to  $\tau_n$  nor the east–west direction. Then, there are eight possible patterns. The subtlety is at the "crossover" of base pairings on the two sides of  $\tau_n$ . In the two rightmost drawings of Figure 15, we observe that if  $n_\alpha$  resides on the left side of  $\tau_n$ , then we have the Bd dynamics similar to that of (1,8) in Figure 12; but if  $n_\alpha$  veers to the right of  $\tau_n$ , then we have the Dd dynamics similar to that of (2,8) in Figure 12. We denote this as a hybrid Bd/Dd base pairing, which results in roundabout behavior near the singular point  $\tau_0$  with distinct traits. Similarly, the Aa/Ca pairing results in a new type of repelling behavior near  $\tau_0$ . Readers might attempt this exercise themselves. Without repeating mundane details, we mention that local patterns, when  $\tau_0$  points in the north–south direction, or even when  $\tau_n$  and  $\tau_0$  are parallel to each other, can be explained by the idea outlined above.

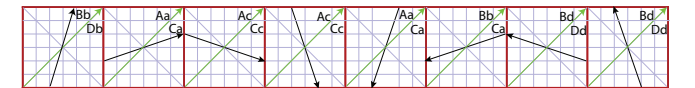


**Figure 15.** Relative positions of  $\tau_0$  and possible transitions of base pairings when  $\tau_n$  points to the northeast.

### 6. Wedged Bases of Scalar-Valued Functions

One simple but significant case must be mentioned because it commonly defies the assumption made in Theorem 1. Consider the surface that is the graph of a first-order continuously differentiable two-variable function  $f: \mathbb{R}^2 \to \mathbb{R}$ . An obvious parametric equation is

$$\begin{cases}
X := x_1, \\
Y := x_2, \\
Z := f(x_1, x_2).
\end{cases}$$
(15)

It is easy to see that

$$\begin{cases}
 n(\mathbf{x}) = \left(\frac{\partial f}{\partial x_2}\right)^2(\mathbf{x}) - \left(\frac{\partial f}{\partial x_1}\right)^2(\mathbf{x}), \\
 o(\mathbf{x}) = 2\frac{\partial f}{\partial x_1}(\mathbf{x})\frac{\partial f}{\partial x_2}(\mathbf{x}).
\end{cases} (16)$$

Thus, singular points  $\mathbf{x}_0$  where  $\mathcal{O}$  and  $\mathcal{N}$  intersect must satisfy  $\frac{\partial f}{\partial x_1}(\mathbf{x}_0) = \frac{\partial f}{\partial x_2}(\mathbf{x}_0) = 0$ . In other words, singular points are precisely the conventional critical points where the gradient of the function f vanishes. Indeed, we find from (10) that the first right singular vector is given by

Mathematics 2023, 11, 3306 17 of 20

$$\mathbf{u}_{1} = \pm \left(1^{2} + \left(\frac{n + \sqrt{n^{2} + o^{2}}}{o}\right)^{2}\right)^{-\frac{1}{2}} \begin{bmatrix} 1 \\ \frac{n + \sqrt{n^{2} + o^{2}}}{o} \end{bmatrix} = \pm \frac{1}{\sqrt{\frac{\partial f}{\partial x_{1}}^{2} + \frac{\partial f}{\partial x_{2}}^{2}}} \begin{bmatrix} \frac{\partial f}{\partial x_{1}} \\ \frac{\partial f}{\partial x_{2}} \end{bmatrix}, \quad (17)$$

so the principal singular curve  $\mathbf{x}_1(t)$  in the context of (15) is precisely the (normalized) gradient flow of  $f(\mathbf{x})$ . The sign choice determines whether this is a descent flow or an ascent flow.

Furthermore, it is clear from (16) that  $o(\mathbf{x})$  and  $n(\mathbf{x})$  are always factorizable in this particular case. We define

$$\begin{cases}
\mathcal{N}^{1} := \{(x,y)|f_{x}(x,y) - f_{y}(x,y) = 0\}, \\
\mathcal{N}^{2} := \{(x,y)|f_{x}(x,y) + f_{y}(x,y) = 0\}, \\
\mathcal{O}^{1} := \{(x,y)|f_{x}(x,y) = 0\}, \\
\mathcal{O}^{2} := \{(x,y)|f_{y}(x,y) = 0\}.
\end{cases} (18)$$

Each critical curve of either  $\mathcal{O}$  or  $\mathcal{N}$  has at least two separate components. So, at a singular point where all components meet together, there will be more than just two intersecting curves (For example, the function  $f(x_1,x_2)=x_1^3-3x_1x_2^2$  has four components for each critical curve  $\mathcal{O}$  or  $\mathcal{N}$ , so at the monkey saddle point, a total of eight critical curves intersect together.). This situation is different from what we have detailed in Figure 12 and Theorem 1. The techniques employed earlier can readily be generalized to this case. However, the multiple components of critical curves allow more variations of sign changes for  $n(\mathbf{x})$  and  $o(\mathbf{x})$  near  $\mathbf{x}_0$ . It is possible to have multiple  $\alpha$  halves for  $\mathcal{N}$  or  $\mathcal{O}$  curves. The following result represents a typical case.

**Lemma 3.** At a singular point,  $\mathbf{x}_0$ , assume that each of the curves defined in (18) contains exactly one curve. Then, up to the equivalence of rotations:

- 1. There are only four possible ways for singular curves to intersect with the N curve, as shown in Figure 16.
- 2. There are only four possible ways for singular curves to intersect with the O curve, as are shown in Figure 17.

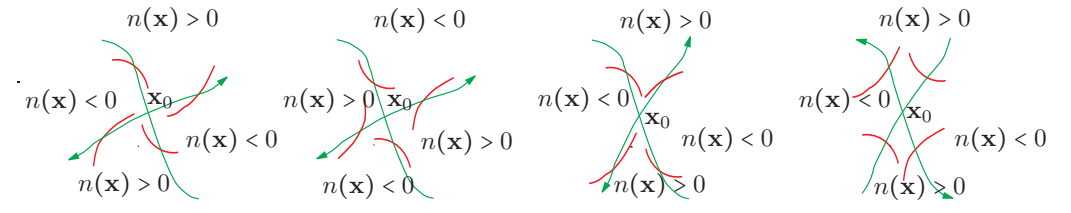


**Figure 16.** Basic concavities of singular curves near  $n(\mathbf{x}) = 0$  for the special case (15).

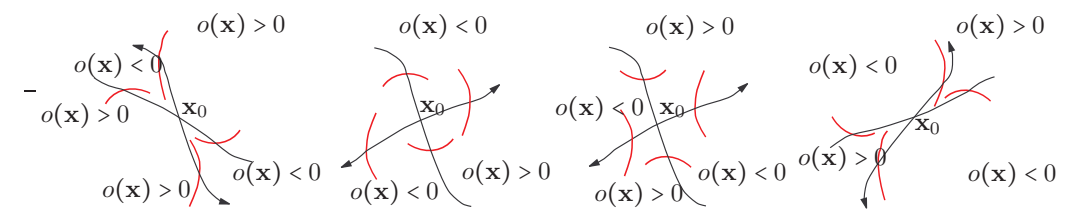


**Figure 17.** Basic concavities of singular curves near  $o(\mathbf{x}) = 0$  for the special case (15).

**Proof.** It can easily be checked that the singular curves cross the critical curves  $\mathcal{N}^1, \mathcal{N}^2, \mathcal{O}^1$ , and  $\mathcal{O}^2$  with tangent vectors parallel to  $\alpha_n$ ,  $\beta_n$ ,  $\alpha_o$ , and  $\beta_o$ , respectively. Trivially, by (17), the tangent of the singular curve is  $\frac{n+\sqrt{n^2+o^2}}{o}$ . It follows that when a singular curve crosses the  $\mathcal{N}$  curve, the absolute value of its tangent becomes greater than one when it enters the region  $\{(x,y)|n(x,y)>0\}$ , and the absolute value of its tangent becomes less than one when it enters the region  $\{(x,y)|n(x,y)<0\}$ . This property necessarily determines the

Mathematics 2023, 11, 3306 18 of 20

concavity of the singular curves. The double-arrow curve in Figure 16 represents  $\mathcal{N}^1$ . There can be only four positions of  $\mathcal{N}^2$  relative to  $\mathcal{N}^1$  that give rise to different local behaviors. Similarly, when a singular curve crosses the  $\mathcal{O}$  curve, its tangent becomes positive when it enters the region  $\{(x,y)|o(x,y)>0\}$ , and its tangent becomes negative when it enters the region  $\{(x,y)|o(x,y)<0\}$ .  $\square$ 

Observe that in each of the eight basic drawings, the property of concavity is symmetric with respect to  $\mathbf{x}_0$ . Therefore, it suffices to identify the corresponding dynamics by simply the upper-half wedge of each drawing. In this way, each wedge is still made of one  $\alpha$ -half and one  $\beta$ -half with a cusp at  $\mathbf{x}_0$ . In Figures 13 and 14, the concavity is determined by one single curve. In contrast, the concavities in the new bases are determined by two curves. These wedged bases give considerably more flexibility for the pairing of  $\mathcal N$  and  $\mathcal O$ . Indeed, we conjecture from our investigation that all 16 pairings are possible.

# 7. Applications

Thus far, we have studied only the motifs of singular curves. The classification of all possible local behaviors suggests a simplistic collection of "tiles" for the delicate and complex "mosaics" observed in the dynamics of singular curves. The inherent characteristics of each given function determine the reflections or kinks of the critical curves ( $\mathcal N$  and  $\mathcal O$ ) and a particular set of base pairings. These local tiles are strung together along the strands of critical curves to form the particular patterns of the underlying functions. While there are zillions of possible variations, we find it interesting that there are only finitely many possible base pairings. To our knowledge, the dynamical system of singular curves has not been studied before. The analysis of such a special differential system should be of theoretical interest in itself.

On the other hand, a successful exploration of the following two questions might help find important applications of the dynamical system of singular curves to parametric surfaces:

- 1. Given a parametric surface, can we decipher the making of its base pairings?
- 2. Given a sequence of base pairings together with a specific formation of critical curves, can we synthesize the main features of a surface?

At present, we are obviously far from completely understanding these concepts. We are hoping that this paper will stimulate further investigation. For the idea to work, it seems plausible to expect that when base pairings are strung together, they form a "gene" which, similar to the biological genes that dictate how the cells are going to live and function, should have the combined effect on determining how a surface would vary. We demonstrate two simple examples below.

**Example 13.** For surfaces arising in the form of (15), the singular points are the critical points and the singular curves are the gradient flows. As expected, the dynamics of singular curves, therefore, trace directions along which function f changes most rapidly. On the one hand, since we allow the integration to go in both forward and backward directions, every gradient trajectory stops at either a local maximum or a local minimum. Depending on the direction of the flows, these kinds of extreme points are either a sink or a source. In contrast to Lemma 2, these singular points are neither propellants nor roundabouts. On the other hand, the only other types of singular points are the saddle points of f, around which the gradient (singular) trajectories will exhibit a mixture of behavior. No Hessian information at the critical point is available unless we fix the sign of the gradient. In all, we believe we have enough knowledge to answer the above two questions in a similar way to how we learn to sketch a surface in multi-variable calculus.

**Example 14.** Critical curves  $\mathcal{N}$  and  $\mathcal{O}$  generally intertwines in a much more involved way. Once their  $\alpha$  halves are determined, which is precisely the inborn property of the underlying function, we begin to see the beauty and complexity of its mosaic patterns. We illustrate our point by color-coding the jigsaw pieces of Example 1 over a small window  $[-2,4] \times [-2,4]$  in Figure 18 to evince the signs of  $n(\mathbf{x})$  and  $o(\mathbf{x})$ . Singular points occur at the common borders where the regions overlap, whose orientations are, thus, determined.

Mathematics 2023, 11, 3306 19 of 20

We look up from Figure 12 to label the singular points with corresponding base pairings. We immediately notice that the same segment of the base parings, say, as short as BbAcBd in the drawing, determines almost the same dynamical behavior, and vice versa. The ideas about sequencing a surface or synthesizing a surface seem sensible.

Although we have all the local pieces in hand, we hasten to point out that there must be some other information missing in the current analysis of the dynamics. For instance, the two groups of singular curves near the point (0,1) in Figure 18 share the same Bd paring and, hence, local behavior. However, when away from this singular point, the singular curves wander off and are contracted to distinct destinations. The long-term dynamics must have other bearings that are not as yet explainable by our local analysis.

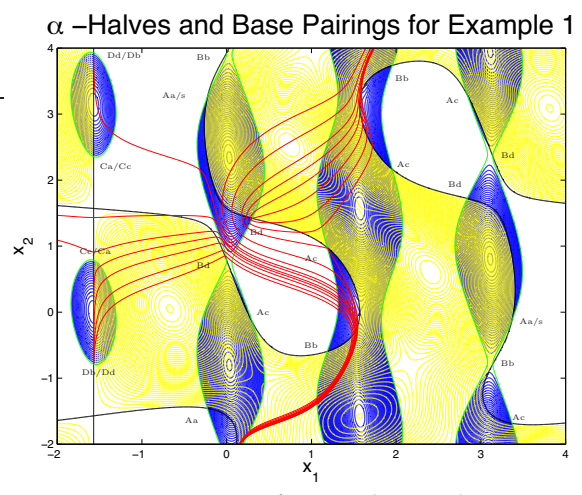


**Figure 18.** Base pairings for sample singular points in Example 1:  $\mathcal{N}$  (green);  $n(\mathbf{x}) > 0$  (blue);  $\mathcal{O}$  (black);  $o(\mathbf{x}) > 0$ , (yellow).

# 8. Conclusions

Gradient adaption is an important mechanism that occurs frequently in nature. Its generalization to Jacobian for vector functions does not immediately reveal the critical adaption directions. That information is manifested by the moving frame formed from the singular vectors of the Jacobian matrix. Intricate patterns resulting from singular curves seem to characterize some underneath movements of the function. The idea discussed in this paper is perhaps the first that relates the dynamical system of singular vectors to parametric surfaces.

The global behavior, in general, and its interpretation in a specific dynamical system of singular vectors, are not yet completely understood. For parametric surfaces in  $\mathbb{R}^3$ , at least, and for any  $f:\mathbb{R}^2\to\mathbb{R}^n$ , in general, this work finds that two strands of curves joined by singular points with specific base pairings make up the local behavior of the function. In particular, at a singular point, where exactly one  $\mathcal N$  curve crosses exactly one  $\mathcal O$  curve, there are exactly eight possible base pairings available.

This work aimed to introduce the notion of singular curves. Many interesting questions remain to be answered, including whether a surface can be genome-sequenced and synthesized.

**Author Contributions:** Conceptualization, M.T.C. and Z.Z.; methodology, Z.Z.; software, Z.Z.; validation, M.T.C. and Z.Z.; formal analysis, M.T.C. and Z.Z.; investigation, M.T.C.; resources, M.T.C.; data curation, M.T.C.; writing—original draft preparation, M.T.C.; writing—review and editing, M.T.C.; visualization, M.T.C.; supervision, M.T.C.; project administration, M.T.C.; funding acquisition, M.T.C. and Z.Z. All authors have read and agreed to the published version of the manuscript.

**Funding:** This research by M.T.C. was supported in part by the National Science Foundation under grants DMS-1912816 and DMS-2309376. This research by Z.Z. was supported in part by the NSFC projects 11071218 and 11971430.

Data Availability Statement: Contact the corresponding author.

Mathematics 2023, 11, 3306 20 of 20

#### **Conflicts of Interest:** The authors declare no conflict of interest.

#### References

1. Golub, G.H.; Van Loan, C.F. *Matrix Computations*, 3rd ed.; Johns Hopkins Studies in the Mathematical Sciences; Johns Hopkins University Press: Baltimore, MD, USA, 1996; pp. xxx+698.

- 2. Stewart, G.W. On the early history of the singular value decomposition. SIAM Rev. 1993, 35, 551–566. [CrossRef]
- 3. Eldén, L. Matrix methods in data mining and pattern recognition. In *Fundamentals of Algorithms*; Society for Industrial and Applied Mathematics (SIAM): Philadelphia, PA, USA, 2007; Volume 4, pp. x+224. [CrossRef]
- 4. Klema, V.C.; Laub, A.J. The singular value decomposition: Its computation and some applications. *IEEE Trans. Automat. Control* **1980**, 25, 164–176. [CrossRef]
- 5. Vandewalle, J.; De Moor, B. On the use of the singular value decomposition in identification and signal processing. In *Numerical Linear Algebra, Digital Signal Processing and Parallel Algorithms (Leuven, 1988)*; NATO Advanced Science Institutes Series F: Computer and Systems Sciences; Springer: Berlin, Germany, 1991; Volume 70, pp. 321–360.
- 6. Wall, M.E.; Rechtsteiner, A.; Rocha, L.M. Singular value decomposition and principal component analysis. In *A Practical Approach to Microarray Data Analysis*; Berrar, D.P., Dubitzky, W., Granzow, M., Eds.; Kluwer: Norwell, MA, USA, 2003; Chapter 5, pp. 91–108.
- 7. Bunse-Gerstner, A.; Byers, R.; Mehrmann, V.; Nichols, N.K. Numerical computation of an analytic singular value decomposition of a matrix valued function. *Numer. Math.* **1991**, *60*, 1–39. [CrossRef]
- 8. Wright, K. Differential equations for the analytic singular value decomposition of a matrix. *Numer. Math.* **1992**, *63*, 283–295. [CrossRef]
- 9. Mumford, D. Curves and Their Jacobians; The University of Michigan Press: Ann Arbor, MI, USA, 1975; pp. vi+104.
- 10. Erdogmus, D.; Ozertem, U. Nonlinear coordinate unfolding via principal curve projections with application to nonlinear BSS. In *Neural Information Processing*; Ishikawa, M., Doya, K., Miyamoto, H., Yamakawa, T., Eds.; Springer: Berlin/Heidelberg, Germany, 2008; pp. 488–497. [CrossRef]
- 11. Hastie, T.J.; Stuetzle, W. Principal curves. J. Amer. Statist. Assoc. 1989, 84, 502-516. [CrossRef]
- 12. Hastie, T.J. Principal Curves and Surfaces. Ph.D. Thesis, Stanford University, Stanford, CA, USA, 1984.
- 13. Kégl, B.; Krzyzak, A.; Linder, T.; Zeger, K. Learning and design of principal curves. *IEEE Trans. Pattern Anal. Mach. Intell.* **2000**, 22, 281–297. [CrossRef]
- 14. Cazals, F.; Faugère, J.C.; Pouget, M.; Rouillier, F. The implicit structure of ridges of a smooth parametric surface. *Comput. Aided Geom. Des.* **2006**, *23*, 582–598. [CrossRef]
- 15. Chern, S.S. Curves and Surfaces in Euclidean space. In *Studies in Global Geometry and Analysis*; Mathematical Association of America: Washington, DC, USA; Prentice-Hall: Englewood Cliffs, NJ, USA, 1967; pp. 16–56.
- 16. Porteous, I.R. *Geometric Differentiation: For the Intelligence of Curves and Surfaces*, 2nd ed.; Cambridge University Press: Cambridge, UK, 2001; pp. xvi+333.
- 17. Dierkes, U.; Hildebrandt, S.; Sauvigny, F. *Minimal Surfaces*, 2nd ed.; Grundlehren der Mathematischen Wissenschaften [Fundamental Principles of Mathematical Sciences]; Springer: Berlin/Heidelberg, Germany, 2010; Volume 339, pp. xvi+688.
- 18. Meeks, W.H., III; Pérez, J. The classical theory of minimal surfaces. Bull. Amer. Math. Soc. 2011, 48, 325–407. [CrossRef]
- 19. de Berg, M.; Cheong, O.; van Kreveld, M.; Overmars, M. *Computational Geometry: Algorithms and Applications*, 3rd ed.; Springer: Berlin/Heidelberg, Germany, 2008; pp. xii+386.
- 20. Gu, X.D.; Yau, S.T. Computational conformal geometry. In *Advanced Lectures in Mathematics (ALM)*; International Press: Somerville, MA, USA, 2008; Volume 3, pp. vi+295.
- 21. Hallinan, P.W.; Gordon, G.G.; Yuille, A.L.; Giblin, P.; Mumford, D. *Two- and Three-Dimensional Patterns of the Face*; A K Peters, Ltd.: Natick, MA, USA, 1999; pp. viii+262.
- 22. Gallier, J. The Classification Theorem for Compact Surfaces and a Detour on Fractals. University of Pennsylvania, 2005. Available online: http://citeseerx.ist.psu.edu/viewdoc/download?doi=10.1.1.133.4358 (accessed on 5 July 2023).
- 23. Gu, D.X.; Zeng, W.; Lui, L.M.; Luo, F.; Yau, S.T. Recent development of computational conformal geometry. In Proceedings of the Fifth International Congress of Chinese Mathematicians. Part 1, 2, Beijing, China, 17–22 December 2010; AMS/IP Stud. Adv. Math. 51, pt. 1; American Mathematical Society: Providence, RI, USA, 2012; Volume 2, pp. 515–560.
- 24. Reuter, M.; Wolter, F.E.; Peinecke, N. Laplace-Beltrami spectra as "Shape-DNA" of surfaces and solids. *Comput.-Aided Des.* **2006**, 38, 342–366; Symposium on Solid and Physical Modeling 2005. [CrossRef]
- 25. Verschelde, J. The Database of Polynomial Systems. University of Illinois at Chicago, 2011. Available online: http://www.math.uic.edu/~jan/demo.html (accessed on 5 July 2023).
- 26. Maclean, A.J. Parametric Equations for Surfaces. University of Sydney, 2006. Available online: https://vtk.org/vtk-in-action/#image-gallery (accessed on 5 July 2023).

**Disclaimer/Publisher's Note:** The statements, opinions and data contained in all publications are solely those of the individual author(s) and contributor(s) and not of MDPI and/or the editor(s). MDPI and/or the editor(s) disclaim responsibility for any injury to people or property resulting from any ideas, methods, instructions or products referred to in the content.